esa

ECOSPHERE

COASTAL AND MARINE ECOLOGY

Survival of the fattest: linking body condition to prey availability and survivorship of killer whales

Joshua D. Stewart[1,†] John W. Durban[2,3] Holly Fearnbach[4] Lance G. Barrett-Lennard,[5] Paige K. Casler,[6] Eric J. Ward[7] and Derek R. Dapp[8]

[1]*National Research Council Postdoctoral Fellow for Marine Mammal and Turtle Division, Southwest Fisheries Science Center, National Marine Fisheries Service, National Oceanic and Atmospheric Administration, La Jolla, California 92037 USA*
[2]*Marine Mammal and Turtle Division, Southwest Fisheries Science Center, National Marine Fisheries Service, National Oceanic and Atmospheric Administration, La Jolla, California 92037 USA*
[3]*Southall Environmental Associates, Aptos, California, USA*
[4]*SR3, SeaLife Response, Rehabilitation and Research, Des Moines, Washington, USA*
[5]*Ocean Wise Conservation Association, Vancouver, British Columbia, Canada*
[6]*Ocean Associates, Arlington, Virginia, USA*
[7]*Conservation Biology Division, Northwest Fisheries Science Center, National Marine Fisheries Service, National Oceanic and Atmospheric Administration, Seattle, Washington 98112 USA*
[8]*Washington Department of Fish and Wildlife, Olympia, Washington, USA*

Citation: Stewart, J. D., J. W. Durban, H. Fearnbach, L. G. Barrett-Lennard, P. K. Casler, E. J. Ward, and D. R. Dapp. 2021. Survival of the fattest: linking body condition to prey availability and survivorship of killer whales. Ecosphere 12(8): e03660. 10.1002/ecs2.3660

Abstract. Recovering small, endangered populations is challenging, especially if the drivers of declines are not well understood. While infrequent births and deaths may be important to the outlook of endangered populations, small sample sizes confound studies seeking the mechanisms underlying demographic fluctuations. Individual metrics of health, such as nutritive condition, can provide a rich data source on population status and may translate into population trends. We examined interannual changes in body condition metrics of endangered Southern Resident killer whales (SRKW) collected using helicopters and remotely operated drones. We imaged and measured the condition of the majority of all three social pods (J, K, and L) in each of seven years between 2008 and 2019. We used Bayesian multi-state transition models to identify relationships between body condition changes and both tributary-specific and area-based indices of Chinook salmon abundance, and *K*-fold cross-validation to compare the predictive power of candidate salmon covariates. We found that Fraser River (tributary-specific) and Salish Sea (area-based) Chinook salmon abundances had the greatest predictive power for J Pod body condition changes, as well as the strongest relationships between any salmon covariates and SRKW condition across pods. Puget Sound (tributary-specific) Chinook salmon abundance had the greatest predictive power for L Pod body condition changes, but a weaker relationship than Fraser River or Salish Sea abundance had with J Pod body condition. The best-fit model for K Pod included no Chinook covariates. In addition, we found elevated mortality probabilities in SRKW exhibiting poor body condition (reflecting depleted fat reserves), 2–3 times higher than whales in more robust condition. Collectively, these findings demonstrate that (1) fluctuations in SRKW body condition can in some cases be linked to Chinook salmon abundance; (2) the three SRKW pods appear to have distinct patterns of body condition fluctuations, suggesting different foraging patterns; and (3) aerial photogrammetry is a useful early-warning system that can identify SRKW at higher risk of mortality in the near future.

Key words: adaptive management; body condition; drones; foraging ecology; multi-state modeling; *Orcinus orca*; photogrammetry; resident killer whale.

Received 4 November 2020; revised 28 February 2021; accepted 8 March 2021; final version received 17 May 2021. Corresponding Editor: Hunter S. Lenihan.

† **E-mail:** joshua.stewart@noaa.gov

Introduction

Endangered species with small population sizes approaching extinction or local extirpation present a diversity of management challenges (Soulé 1987, Dennis 1989). When the causes of population declines are not well established, it is difficult to identify management strategies that will prevent declines and promote recovery. Studies of small populations by definition suffer from sample size limitations (Walsh 2000, Brosi and Biber 2009), complicating efforts to identify stressors that may be influencing population trends (Schönbrodt and Perugini 2013). For example, infrequent births or deaths may have dramatic impacts on population trends, but may be too sparse to identify mechanisms. In these cases, non-invasive metrics of individual health can help identify drivers of population trends and allow for management strategies that preempt demographic casualties that impact population viability, such as the loss of reproductive females.

Nutritive condition in long-lived vertebrates can provide a sensitive signal of short-term individual or population health. Changes in condition may reflect changes in the environment or foraging success, and persistent variation may translate into population trends (Berger 2012, Boulanger et al. 2013, Vindenes et al. 2014). Aerial imaging technology has provided one example of such non-invasive individual health metrics (Perryman and Lynn 2002). Photogrammetry with remotely controlled drones has been used increasingly over the past 5–10 yr as drones have become cheaper, safer, and more efficient compared with traditional photogrammetry using crewed aircraft (Durban et al. 2015). These methods have been widely applied to both terrestrial and marine species (Goebel et al. 2015, Hu et al. 2020). Working with marine or other aquatic organisms is particularly challenging, as individuals are highly mobile and may spend little time near the surface where they can be imaged. Nevertheless, aerial photogrammetry has been used to collect individual measurements of marine mammal species including investigations of life-history characteristics (Christiansen et al. 2016, Groskreutz et al. 2019) and nutritive condition (Christiansen et al. 2018, Fearnbach et al. 2018, 2020). A strength of aerial photogrammetry is that it can non-invasively provide quantitative metrics of body condition at the individual level (Durban et al. 2015, Fearnbach et al. 2018), which can be used to evaluate the health or status of a large portion of a population in near real time. These high-resolution measures of condition and fitness may in turn contribute to an understanding of the mechanisms underlying demographic variability, for example, by linking condition to reproductive success (Christiansen et al. 2016) or mortality (Christiansen et al. 2020).

Collecting individual health data from wild populations may be challenging, particularly if individuals cannot be identified or the population is not censused. Killer whales (*Orcinus orca*) represent an ideal case for relating individual health metrics to the environment, as population sizes are typically small, and individuals are readily identifiable. One of the smallest populations of killer whales, the Southern Resident killer whale (SRKW) population, is censused annually and demographic characteristics (age, sex) have been recorded for the entire population since the mid-1970s (Center for Whale Research 2020). This small ($n = 73$) population of fish-eating killer whales is found in the eastern north Pacific (Ford et al. 1998) with a range including coastal waters from central California to Southeastern Alaska, and core summer habitat in the Salish Sea between Puget Sound and Southern Vancouver Island (National Marine Fisheries Service 2019). Because of its small size and a decline in abundance of approximately 25% since 1995, the SRKW population is listed as endangered under the Endangered Species Act (ESA) in the United States and the Species-at-Risk Act (SARA)

in Canada. The diet of SRKWs comprises primarily Chinook salmon (*Oncorhynchus tshawytscha*), although other species such as Coho salmon (*Oncorhynchus kisutch*), chum salmon (*Oncorhynchus keta*), halibut (*Hippoglossus stenolepis*), and groundfish have also been identified in their diets (Hanson et al. 2010, Ford et al. 2016). Three main stressors are thought to be responsible for SRKW population declines: (1) elevated levels of environmental pollutants in their core habitat range that could impact survivorship and reproductive success (Krahn et al. 2009); (2) increasing vessel noise and disturbance in the Salish Sea which could interfere with communication and foraging efficiency (Lusseau et al. 2009); and (3) declining Chinook salmon populations and therefore prey scarcity (Ford et al. 2010), which in addition to direct effects could compound the other stressors (e.g., Lundin et al. 2016).

Several studies have supported the hypothesis that prey limitation is a primary threat to the SRKW population, linking aggregates of Chinook salmon abundance to both fecundity and mortality (Ward et al. 2009, Ford et al. 2010, Vélez-Espino et al. 2014, Wasser et al. 2017) as well as to declines in adult body size (Fearnbach et al. 2011, Groskreutz et al. 2019). However, the range of both SRKWs and their salmon prey is enormous, encompassing over 3000 km of coastline, and identifying the prey populations that are most important for SRKWs is challenging. Chinook salmon face a complex suite of stressors including habitat modification and degradation (Greene and Beechie 2004), restricted access to spawning tributaries (Sheer and Steel 2006), fisheries pressure (Ruckelshaus et al. 2002), increased natural mortality due to recovering marine mammal populations (Chasco et al. 2017), variable at-sea survival (Losee et al. 2019, Welch et al. 2021), and climate impacts (Crozier et al. 2008). Chinook populations from four tributaries within the SRKW range are themselves listed as endangered in the United States or Canada, with several others listed as threatened. To date, no studies have been able to identify relationships between specific salmon populations and SRKW survivorship or population health (Pacific Fishery Management Council 2020).

Aerial photogrammetry can provide a precise measure of individual killer whales' nutritive condition by quantifying the relative amount of adipose fat stored behind the cranium; as individuals decline in nutritive condition, they metabolize adipose fat in addition to blubber stores (Fearnbach et al. 2020). As such, photogrammetry datasets potentially provide more power to evaluate relationships between prey abundance and population status compared with efforts to link prey to infrequent births and deaths. In this study, we used aerial photogrammetry images of individually recognizable SRKWs collected in 7 September field efforts across 12 yr (2008–2019) to evaluate how changes in body condition might be related to the abundance of different Chinook salmon populations. The SRKW population is composed of three distinct collections of matrilineal family units (hereafter referred to as J, K, and L pods; Parsons et al. 2009), and we considered each pod separately in our analyses based on previously described differences in range and movement patterns (National Marine Fisheries Service 2019, Riera et al. 2019).

Methods

Data collection

Aerial images of Southern Resident killer whales were collected in the Salish Sea near the San Juan Islands, WA (Fearnbach et al. 2011, Groskreutz et al. 2019) in the month of September in each of seven years. Images were collected from a manned helicopter in 2008 and 2013 (Fearnbach et al. 2011, 2018) and using a drone in 2015–2019 (Durban et al. 2015, Fearnbach et al. 2020). Briefly, vertical images were collected using a digital camera at altitudes of 230–460 m by helicopter and 25–45 m by drone. Despite changes in aircraft platforms, all images were obtained with a Normal lens to ensure a flat image with no wide-angle distortion, with the specific camera and lens chosen based on aircraft altitude to achieve a water-level pixel resolution of 1–2 cm (Durban et al. 2015). Research activities were permitted by the National Marine Fisheries service in the U.S. and the Department of Fisheries and Oceans in Canada, and aerial photogrammetry was approved as an observational (non-invasive) method by the Institution Animal Care and Use Committee of the NOAA Southwest Fisheries Science Center Marine Mammal and Turtle

Division. Individual whales can be identified by unique markings that are visible from aerial images, allowing measurements to be linked to individual whales of known age and sex (Fearnbach et al. 2011, 2020, Durban et al. 2015). As a quantitative metric of body condition, we used the eye patch ratio (EPR), which is the ratio of the pixel distance between the inside of the white eye patch pigmentation at their anterior end relative to their distance at 75% of the eye patch length, described in Fearnbach et al. (2020; Fig. 1). The eye patch ratio is a sensitive metric of nutritive condition as it measures the relative amount of adipose fat stored behind the cranium. As killer whales become nutritionally stressed, they lose this adipose tissue along with blubber fat reserves, resulting in lower EPRs, and as such, this is a more sensitive metric of nutritive condition in killer whales compared to other commonly used metrics such as head width to body length ratios (Fearnbach et al. 2020). Multiple measurement-quality images were available of a single whale on a given day and within years, and we used the mean EPR for each whale in each year because EPR calculations had very low variability (e.g., typical coefficients of variation of 0.003–0.008 for within-year variability of a given whale; Fearnbach et al. 2020).

Accounting for age and sex

To prepare the raw eye patch ratio data for analysis, we first fit a generalized additive model to the EPRs using the mgcv package (Wood 2006) in R (R Core Team 2016) to account for expected variability in nutritive condition and EPRs by age and sex. Age and sex data were available from long-term demographic modeling efforts (Center for Whale Research 2020). We fit separate smooth terms to male and female EPRs from whales aged 0–60 (Fig. 1). We used the raw residuals (observed EPR minus mean EPR estimated by the spline fit) as the basis for defining body condition classes. Ages of a few mature Southern Resident killer whale females that were reproductive when monitoring began in the 1970s are not known precisely, so we calculated residuals for those whales by subtracting observed EPRs from the mean EPR of whales age 60+. We aggregated the residuals of all EPR measurements from all pods across all years and split that distribution into five equal quantiles, representing the age- and sex-normalized body condition classes to be used in the multi-state model, with body condition class 1 (BC1) being the lowest 20% quantile and BC5 being the highest 20% quantile. Finally, we created a matrix of individuals' body condition classes by year, including unsampled years 2009–2012 and 2014. In unsampled years, and in years where a whale was not photographed despite survey effort, individual condition was logged as NA. Known deaths from the annual census (Center for Whale Research 2020) were also included in the matrix to facilitate estimation of both age/sex- and body condition-specific mortality probabilities. Because photogrammetry data were collected in September of each year, we considered deaths that occurred between October and the following September to belong to the following survey year. For example, if a whale was measured in September 2016 and died in November 2016, we logged that death in the following time step of the condition matrix, 2017, to allow the model to account for the transition from the condition measured in September 2016 to death. Two known anthropogenic-related deaths were not included in the model: whale J34 died of blunt force trauma in 2016 (Raverty et al. 2020) and was measured in body condition class 5 the same year; L95 died in 2016 of a fungal infection that may have been associated with a satellite tag attachment (Huggins et al. 2020) and was measured in body condition class 1 the previous year. The condition matrix for those whales was left as unknown (NA) after their last measurements, to prevent them from influencing mortality probabilities for their respective body condition classes prior to death.

Statistical model

We developed a Bayesian multi-state modeling framework to evaluate changes in body condition between years and the probability of mortality of different condition classes, after accounting for differences in mortality by age and sex. All modeling was performed in JAGS via R (Plummer 2003) and built upon previous multi-state modeling approaches (Kery and Schaub 2012). The model estimated annual transition probabilities between body condition classes, as well as transitions from each body condition class to death, which are the condition-specific mortality

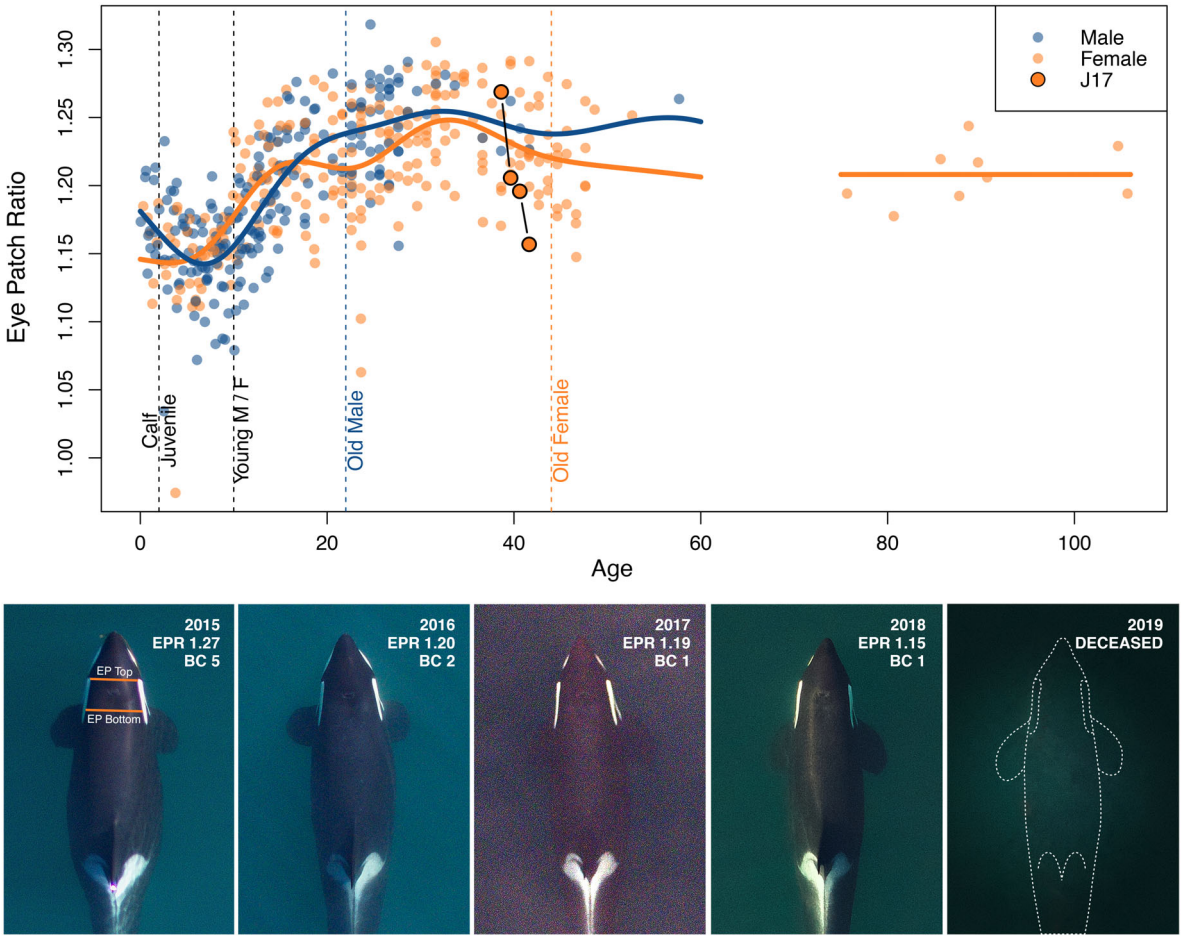

Fig. 1. Eye patch ratios by age and sex for Southern Resident killer whale individuals from all three pods during the study period. The top panel shows the measured eye patch ratio by age for males (blue) and females (orange). The spline fits for males (blue) and females (orange) were used to define body condition classes based on residuals, while a mean eye patch ratio was used to calculate residuals for females aged 60+ that did not have reliable age estimates (see Methods). Vertical dashed lines delineate the age and sex classes used to estimate age- and sex-specific mortality probabilities. The series of images tracks the eye patch ratio (EPR) and body condition class (BC) of adult female J17 from 2015 to 2018, demonstrating the observed decline in condition preceding her death in summer 2019. The progression of J17's eye patch ratios is highlighted in the top panel in larger, dark orange circles connected by lines. The orange horizontal lines in the far-left image show how the eye patch ratio is calculated (EP bottom divided by EP top), providing a metric of adipose fat behind the cranium as a proxy for nutritive condition.

probabilities. An increase of one condition class (e.g., BC 1–BC 2; BC 3–BC 4) was considered growth (G). Increases of two or more condition classes were considered multiple single Growth steps, and their probabilities were therefore exponentiated (e.g., BC 1–BC 3 = G^2; BC 1–BC 4 = G^3). Remaining in the same condition class in two sequential years was considered stable (S). A decrease of one condition class was considered decline (D), and decreases of two of more condition classes were exponentiated as with growth transitions. The advantages of using power functions for the G and D elements are that the number of parameters is reduced relative to an unconstrained matrix, and transitioning across multiple steps is constrained to be less likely than

transitioning a single step. In order to make population-level inferences from individual changes in condition, all animals transitioning in the same direction and magnitude contributed to the same transition probabilities, regardless of their starting condition class:

	BC1	BC2	BC3	BC4	BC5	Dead
BC1	S_t	G_t	G_t^2	G_t^3	G_t^4	$M_{1_{i,t}}$
BC2	D_t	S_t	G_t	G_t^2	G_t^3	$M_{2_{i,t}}$
BC3	D_t^2	D_t	S_t	G_t	G_t^2	$M_{3_{i,t}}$
BC4	D_t^3	D_t^2	D_t	S_t	G_t	$M_{4_{i,t}}$
BC5	D_t^4	D_t^3	D_t^2	D_t	S_t	$M_{5_{i,t}}$
Dead	0	0	0	0	0	1

where rows are the condition class in year $t - 1$, columns are the condition class in year t, and the matrix is populated by transition probabilities for year t. To make the sum of each row equal to 1, we normalized each row by dividing each element by its row sum (e.g., Cobb and Chen 2003, Liu et al. 2008). Mortality probabilities M were dependent on an individual whale's age, sex, and body condition. As a result, differences in mortality probability based on age, sex, and body condition slightly affected transition probabilities during row normalization. This can be interpreted as making transition probabilities between condition classes conditional upon a whale surviving.

Mortality probability was estimated in two steps: first based on the age and sex of a whale and then based on the condition class of that whale. We assigned an age class to each whale at each time step in the model, following previous classifications used for SRKW demographic modeling (Ward et al. 2013). Both males and females age 0–2 were defined as calves and 2–10 as juveniles. Females age 10–44 were defined as young females and 45+ as old females. Males age 10–22 were defined as young males and 23+ as old males (Fig. 1). The baseline mortality probability for whales in each age class was defined as:

$$M_{\text{Base}_a} \sim N[\text{logit}(\widehat{M}_{\text{Base}}), \sigma]$$

$$\widehat{M}_{\text{Base}} \sim U[0, 1]$$

where M_{Base} is the baseline mortality probability for a whale in age class a (of the 6 age/sex classes defined above), which is normally distributed around the overall mean mortality probability, $\widehat{M}_{\text{Base}}$, with variance σ in logit space. We then added a random effect of body condition such that the mortality probability of a whale at a given time step was calculated as:

$$M_{i,t} = \text{inv.logit}(M_{\text{Base}_{i,t}} + M_{\text{bc}_{i,t}})$$

$$M_{\text{bc}} \sim N[0, \sigma]$$

where M is the mortality probability (in proportional space) for whale i at time t, M_{Base} is the age-specific baseline mortality probability (in logit space) for whale i given its age and sex class at time t, and M_{bc} is the condition-specific effect (in logit space) on baseline mortality for whale i given its body condition class bc at time t. M_{bc} for body condition class bc (1–5) is normally distributed around zero with variance σ in logit space. After applying the random effect of body condition to the whale's baseline mortality probability, that sum is converted to proportional space using the inverse logit transformation.

To incorporate salmon abundance covariates into the model, we used a cumulative logit transformation to allow covariates to have independent relationships to growth and decline transition probabilities while remaining bounded by [0, 1] in proportional space. For growth and decline transitions, we used the following equation:

$$\text{Transition}_{c,t} = e^{\text{intercept}_c + \text{slope}_c \times \text{covariate}_t + \varepsilon_{c,t}}$$

where Transition is the uncorrected transition probability in cumulative logit space of transition type c (i.e., G or D) at time t, intercept and slope are the linear relationship terms for each transition type c, covariate is the salmon index at time t, and ε is the residual error around the linear fit for transition type c at time t, with

$$\varepsilon_{c,t} \sim N[0, \sigma]$$

where the ε terms for each transition type c are normally distributed around zero with variance σ. In the cumulative logit transformation, one parameter must be fixed at 1 for identifiability, which we applied to the probability of stable condition (S):

$$\text{Transition}_{S,t} = 1$$

The uncorrected transition probabilities are then transformed to proportional space so that they are bounded by [0, 1]:

$$\text{Prob}_{c,t} = \frac{\text{Transition}_{c,t}}{\sum_i \text{Transition}_t}$$

where Prob is the corrected probability for each transition type c (G, D, and S) at time t.

Missing values of condition classes (included as NA in the condition matrix) were estimated by the model as part of the joint posterior distribution and were treated as an unknown model parameter or latent state. As the number of consecutive missing values for an individual whale increases, the uncertainty in the posterior estimates of those condition classes is also expected to increase, as there will be more plausible condition sequences to link the observed conditions on either side of the missing values. Because the model requires condition classes in two consecutive years in order to estimate a transition probability, this approach allowed us to include data from whales with incomplete measurement histories (and span the field sampling gap from 2009 to 2012) by using the model to probabilistically assign missing condition classes based on estimated covariate relationships and condition data before and after missing values.

Salmon covariates

We evaluated seven different Chinook salmon abundance indices to identify potential relationships between SRKW body condition and prey availability. We only considered Chinook salmon given the reported importance of Chinook to SRKW life history and reproductive success (Ward et al. 2009, Ford et al. 2010). We used estimates of Chinook salmon abundance from a model used to manage salmon harvest (Fishery Regulation Assessment Model; FRAM; Pacific Fishery Management Council 2008). The FRAM model estimates the abundance of multiple west coast salmon populations (or stocks) available to fisheries, and its outputs were recently synthesized with Chinook spatiotemporal distribution models to generate indices of Chinook available to killer whales by area, year, and season (Pacific Fishery Management Council 2020).

We used three tributary-specific and four area-specific Chinook indices (Pacific Fishery Management Council 2020). In this framework, estimates of Chinook are generated by season, corresponding to the seasons in the FRAM model (October–April, May–June, July–September). For all analyses, we used estimated starting abundances on July 1st of each year, representing abundance at the beginning of the summer season. SRKW are imaged in September each year, so this summer index of abundance provides the closest match to the true prey availability experienced by whales prior to condition measurements. Furthermore, condition at the time of measurement is unlikely to represent the availability of prey more than a few months prior, as SRKW condition is known to fluctuate seasonally, presumably in response to foraging opportunities (Fearnbach et al. 2020). We focused on three of the larger tributary-specific indices (Fraser River, Columbia River, and Puget Sound) and included all modeled stock abundances originating from those tributaries (Appendix S1: Table S1). We note that there is no spatial component to the tributary-specific indices. The four area-specific indices we used were North of Cape Falcon (NOF), Oregon (OR), the Salish Sea (Salish), and Southwest Vancouver Island (SWVI) (Pacific Fishery Management Council 2020). These area-specific indices summed the model estimated abundances of all Chinook salmon from all index stocks that were estimated to be present.

Transition probabilities within the model were related to the salmon index of the year that the whales were transitioning into. For example, the probability of growth (G) from condition class in September 2014 to condition class in September 2015 was linked to estimated Chinook abundance in the summer season (starting July 1st) of 2015. Given the observed differences in body condition trends between SRKW pods, we ran J, K, and L pods through the model separately, each with the same seven candidate covariates to identify potential relationships between each pod and various salmon indices. To determine whether there was support for the inclusion of covariates on transition probabilities, we also considered a null model (condition transition probabilities fixed across all years) and a time-only model (condition transition probabilities estimated independently each year with no covariate). Given the relatively small number of deaths that occurred during the study period, and previous studies that have assumed shared mortality probabilities across pods (Ward et al. 2013), we also ran null and time-only models for all pods combined to estimate population-wide

mortality probabilities with body condition effects. For each model, we ran three chains of 100,000 iterations each, with a burn-in of 50,000 iterations and thinning of 50 for a total of 3000 samples from the posterior distribution. We used non-informative uniform priors for all parameters (Mitchell and Beauchamp 1988) and confirmed model convergence using potential scale reduction factors (Gelman and Rubin 1992; all parameters PSRF < 1.05) and visual inspection of chain convergence.

Model selection

To identify which (if any) Chinook salmon covariates best predicted SRKW body condition transitions, we used a *K*-fold cross-validation approach (Vehtari et al. 2017). There are many different ways to split training and test data sets for cross-validation, depending on the goals of inference. Because our focus is on the temporal aspect, and in developing tools for making short-term future predictions of body condition, we treated data from each year iteratively as a fold. For each pod and covariate combination, we ran the multi-state condition transition model once with each year of observed condition data held out ($n = 7$ yr), using the remaining years of observed condition data to fit the estimated condition transition probabilities and covariate relationships. We then calculated the expected log pointwise predictive density (ELPD) across all held out years of observed body conditions based on the conditions in the previous year and the model-estimated transition probabilities, following (Vehtari et al. 2017). We performed *K*-fold cross-validation for each of the pod and covariate combinations, as well as for each pod with the null and time-only models described above. In addition to the computing the ELPD for each model (models with the highest ELPD receive the highest data support), we calculated the standard error, which is useful in quantifying the uncertainty associated with model selection (Vehtari et al. 2017).

Results

In the seven sampled years between 2008 and 2019, a total of 473 measurements of body condition were collected from 99 whales, which were used in our analyses. We recorded a median of 5 yr of body condition measurements for each whale (range 1–7). A total of 47 deaths and 33 births were documented in SRKWs between 2008 and 2019, while a total of 29 deaths and 15 births were documented in SRKWs during the same 7 yr as the aerial photogrammetry sampling (Center for Whale Research 2020).

In general, *K*-fold cross-validation from our Bayesian models suggested that killer whale body condition is better predicted when salmon covariates are included, relative to models without salmon (J and L pods, Appendix S1: Table S2). For models with salmon included, the standard errors of the ELPD values exceeded the difference in ELPD values among candidate models, which makes it challenging to confidently select one best-fit model. The high standard errors are likely due to having only seven years of condition data with which to calculate ELPDs, given that we considered an entire year of condition data to be a fold. Consequently, we also report the second best-fit model for each pod (Appendix S1: Figs. S1–S3). Due to the complexities of our model and the number of parameters, we present both the raw estimated transition probabilities and aggregated Stable and Growth transition probabilities. This grouping represents a positive transition group that may be more useful for managers targeted at preventing condition declines and maintaining stable or increasing condition.

Fraser River Chinook was the best predictor of J pod condition transitions (Fig. 2, Appendix S1: Table S1), although the ELPD value of the Salish Sea area-based Chinook abundance model fit (which includes a large proportion of the Fraser River stock) was almost identical. J Pod had a significant negative relationship between Fraser River Chinook abundance and the probability of declining condition (Decline), with 95.3% of posterior draws for the slope term in the cumulative logit regression < 0. There was no clear relationship between Fraser River Chinook abundance and the probability of increasing condition (growth; 38.5% of posterior draws > 0), and while the probability of stable condition appears to have a positive relationship with Fraser River Chinook, a slope term for S is not explicitly calculated in the cumulative logit regression. However, as the sum of the probabilities of growth and stable condition is equal to 1 minus the

probability of decline, we can infer that there is a positive relationship between Fraser River Chinook and positive condition transitions (growth or stable condition; Fig. 2). When Fraser River Chinook salmon abundance was above 750,000 fish, J pod whales had a >0.86 median probability of stable or increasing condition. That probability decreased at lower Fraser River Chinook abundance, to a minimum 0.37 median probability of increasing or stable condition when Fraser River Chinook abundance fell to 347,000 fish.

The best-fit model for L pod included Chinook Salmon from Puget Sound, and nearly all models with salmon included outperformed the null models (Appendix S1: Table S1). There was moderate support for a negative relationship between Puget Sound Chinook abundance and the probability of declining condition, with 88% of posterior draws for the slope < 0. Similar to the results for J pod, there was no clear relationship between this index of salmon abundance and the probability of increasing condition (56.9% of posterior draws > 0). Nevertheless, when Puget Sound Chinook abundance was above 399,000 fish during the study period, L pod whales had a 0.82–0.89 median probability of stable or increasing condition. At the second-lowest Puget Sound Chinook abundance during the study period, 235,000 fish in 2015, L pod whales had a 0.32 median probability of stable or increasing condition. The major deviation from the positive linear relationship between Puget Sound Chinook abundance and condition transitions occurred in 2014, when Puget Sound Chinook was at its lowest point during the study period (208,000 fish), but L pod whales had a 0.60 median probability of stable or increasing condition. Apart from Puget Sound Chinook, all other models for L pod that included salmon covariates (both tributary-specific and area-based abundance) produced potentially spurious results, where higher salmon abundance was associated with declining condition (e.g., Appendix S1: Fig. S3).

Unlike J and L pods, the best-fit model for K pod did not include salmon as a covariate, and transition probabilities were held constant across years. In this null model, the median fixed probability of increasing condition (growth) was 0.40 (95% highest posterior density intervals [HPDIs]: 0.33–0.47). The median probability of decline was 0.31 (0.25–0.37), and the median probability of stable condition was 0.29 (0.21–0.38). The second best-fit model for K pod included Puget Sound Chinook abundance, although we note that this covariate relationship produced relatively constant condition transitions across years (Appendix S1: Fig. S2). Nevertheless, there was a significant positive relationship between Puget Sound Chinook abundance and the probability of increasing condition, with 94.93% of posterior draws for the slope > 0. There was no clear relationship between Puget Sound Chinook abundance and the probability of declining condition (22.6% of draws <0), and the probability of stable condition decreased with increasing Chinook abundance (Appendix S1: Fig. S2). When Puget Sound Chinook abundance was above 399,000 fish, K pod whales had a median 0.43–0.50 probability of increasing condition. In contrast, when Puget Sound Chinook abundance was at a low of 208,000, K pod whales had a median 0.14 probability of increasing condition. However, the probability of the management-relevant combined growth and stable condition remained relatively constant across the study period (median 0.68–0.78 probability; Appendix S1: Fig. S2).

While observations of body condition provided a relatively large sample size for estimating transition probabilities, deaths were relatively uncommon during the 12-year study period. Consequently, we estimated the effects of age, sex, and body condition on mortality probabilities by pooling all pods together and running models without covariates (null and time-only). There were 25 total deaths of whales that also had measurements of body condition in at least one year during the study period (12 in J pod, 3 in K pod, and 10 in L pod). 15 of those deaths occurred in the time step immediately following a body condition measurement. With data from all pods combined, the null model had a higher ELPD score than the time only model (Appendix S1: Table S1) and was therefore used for estimates of mortality probability. The median expected mortality probabilities for whales in each age/sex and body condition class are reported in Table 1. The estimated mortality probability of whales in body condition class 1 was 2–3 times higher than other body condition classes (Fig. 3, Table 1). Mortality probability decreased in condition class 2, was lowest in condition classes 3 and 4, and increased slightly in

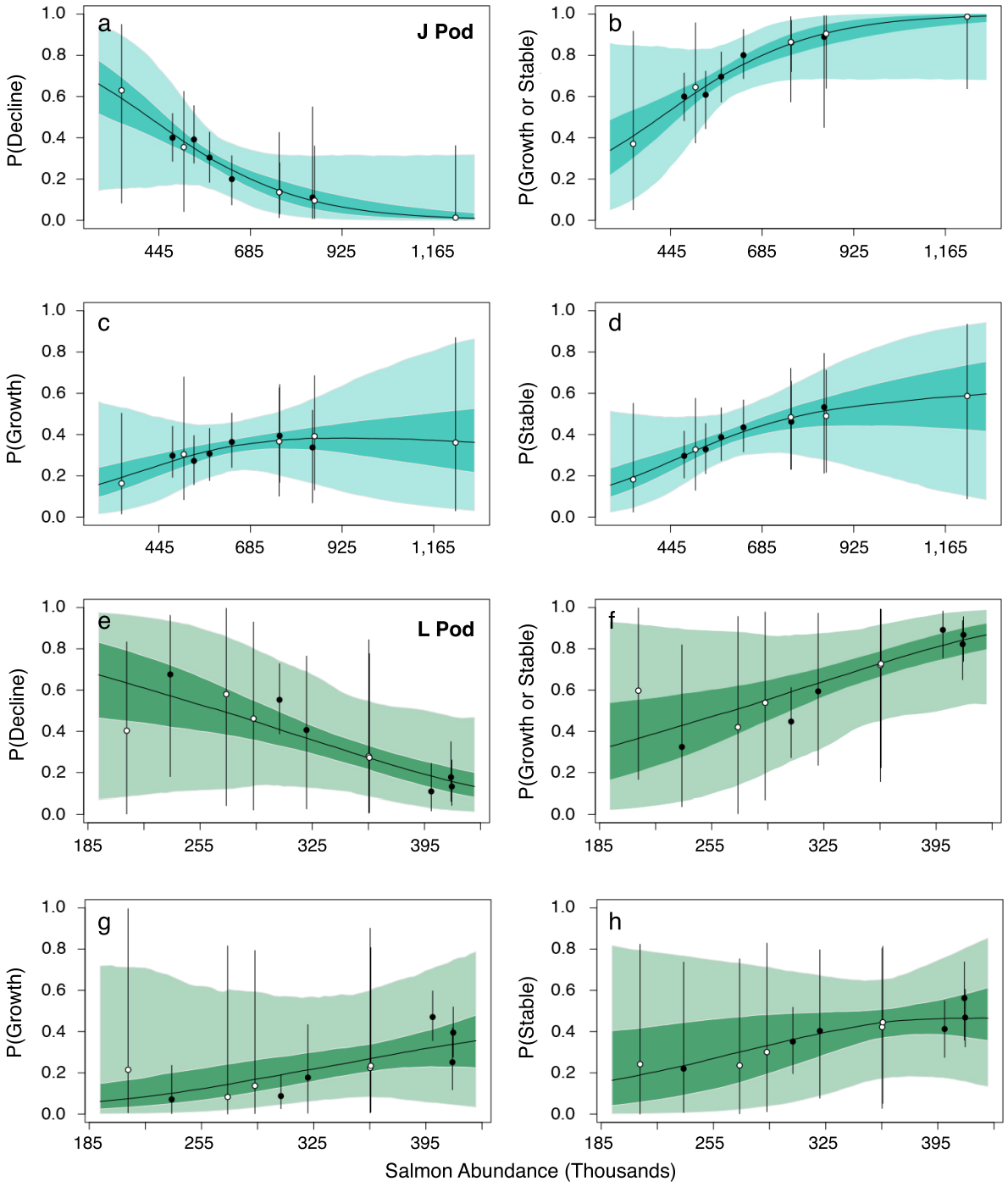

Fig. 2. Body condition transition probabilities for Southern Resident killer whale J (a–d) and L (e–h) pods with best-fit Chinook salmon covariates (Fraser River a–d and Puget Sound e–h). The best-fit model for K pod did not include a covariate (see Results). Panels show the model-estimated relationships between Chinook salmon abundance and the probability of a Decline in body condition (a, e), and the combined probability of Growth or Stable body condition (b, f). The probability of Growth or Stable condition shown in b and f is the sum of the posterior distributions for the probability of Growth (c, g) and the probability of Stable condition (d, h). Put simply,

(Fig. 2. *Continued*)

b = c + d and f = g + h. Points and vertical bars represent the median estimated transition probability with 95% Highest Posterior Density Intervals. White circles indicate years with no photogrammetry measurements when condition classes were estimated by the model. The light and dark shading represent the 95% and 50% HPDIs, respectively, of the model-estimated relationship between salmon covariates and transition probabilities, along with the median estimate of this fit (black line).

Table 1. Model-estimated mortality probabilities by body condition (BC) and age/sex class for Southern Resident killer whales.

Age/sex class	BC 1	BC 2	BC 3	BC 4	BC 5
Calf	0.04	0.02	0.01	0.01	0.02
	(0.004–0.177)	(0.001–0.085)	(0.001–0.066)	(0.001–0.069)	(0.002–0.105)
Juvenile	0.02	0.01	0.01	0.01	0.01
	(0.003–0.060)	(0.001–0.030)	(0.000–0.025)	(0.000–0.025)	(0.002–0.037)
Young female	0.03	0.01	0.01	0.01	0.02
	(0.009–0.081)	(0.003–0.043)	(0.001–0.033)	(0.001–0.033)	(0.005–0.048)
Old female	0.23	0.12	0.08	0.09	0.14
	(0.069–0.595)	(0.026–0.348)	(0.010–0.261)	(0.011–0.274)	(0.042–0.406)
Young male	0.03	0.01	0.01	0.01	0.02
	(0.006–0.105)	(0.002–0.052)	(0.001–0.039)	(0.001–0.041)	(0.003–0.062)
Old male	0.16	0.08	0.05	0.06	0.09
	(0.047–0.432)	(0.018–0.231)	(0.006–0.171)	(0.007–0.173)	(0.026–0.267)

Note: Reported values are median estimates of the probability of mortality in a one-year time step, with 95% highest posterior density intervals in parentheses.

condition class 5 to levels similar to condition class 2. For example, based on the model estimates, a Young Female whale has expected mortality probabilities of: BC1 0.03 (0.009–0.081); BC2 0.014 (0.003–0.043); BC3 0.009 (0.001–0.033); BC4 0.01 (0.001–0.033); BC5 0.017 (0.005–0.048). Of the whales that died during the study period, condition class 1 whales died soonest after their final condition measurement (mean 169 days), while the time between measurement and estimated death roughly increased with condition class: mean 456, 790, 572, and 905 days for classes 2–5, respectively (Fig. 4).

Discussion

The Southern Resident killer whale population offers a unique study opportunity for individual-based body condition monitoring, providing a robust framework that can be extended to other marine and terrestrial populations. Due to the small population size, intensive demographic monitoring, and known fates of virtually every individual, paired with annual photogrammetry measurements of most of the population, we were able to make direct estimates of the relationship between individual salmon stocks and SRKW condition, and relate condition to survival probability. While small demographic fluctuations limit statistical power for identifying the influence of covariates such as prey abundance, aerial photogrammetry allows for more individuals to be sampled in each year and repeatedly sampled across years, increasing power to evaluate changes in body condition against possible drivers. In this case, we obtained more than ten times as many observations of body condition as observations of births and deaths in the seven years of data collection. While our time series of condition measurements was relatively short, we posit that with continued annual monitoring this method will provide sufficient statistical power for even finer scale investigations of prey availability and population status (e.g., at the individual stock level rather than tributary-level aggregates). Evaluating changes in body condition over time likely provides more insights into drivers of population health than simply comparing single measures of condition (e.g., annual population mean and variance) to potential

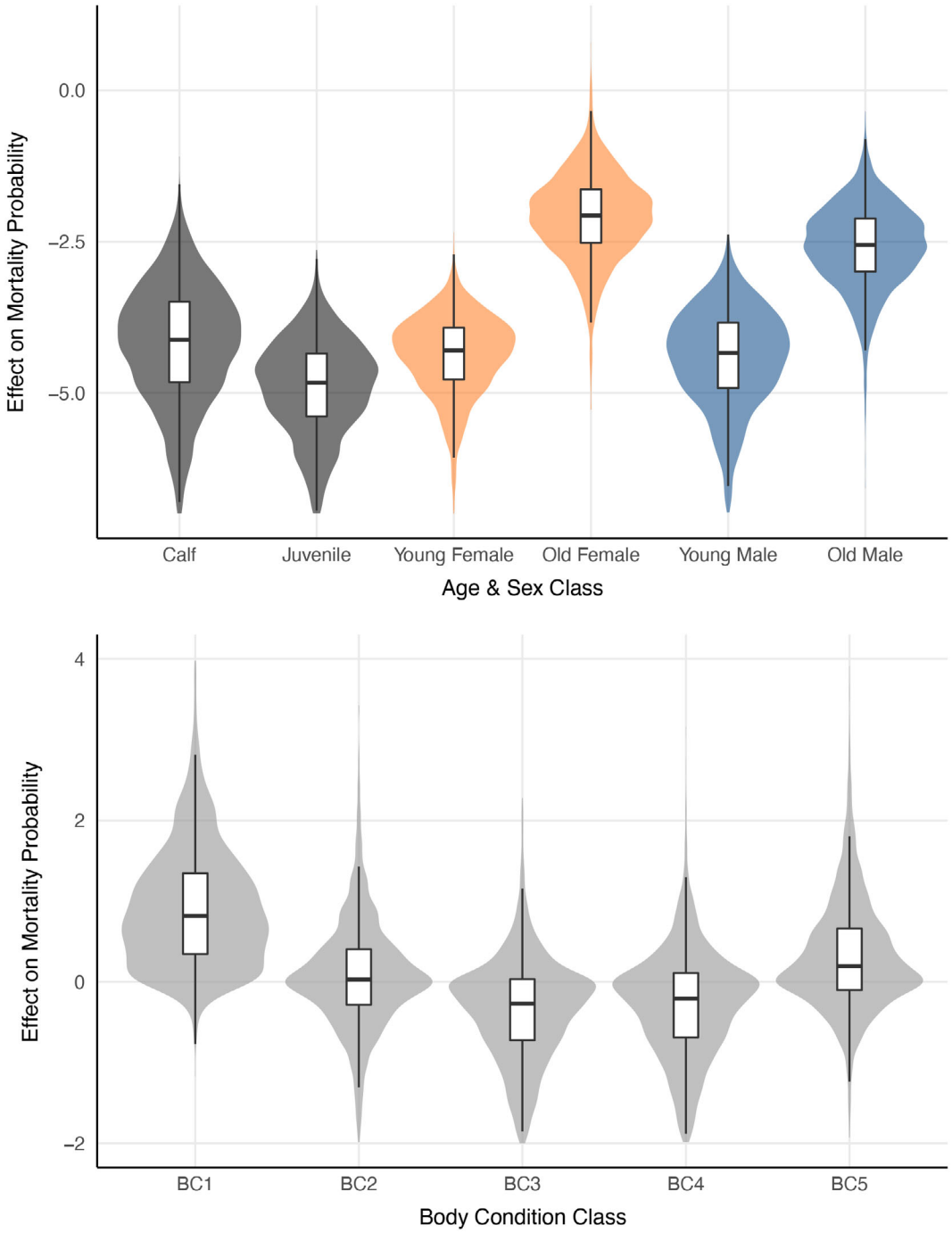

Fig. 3. Age/sex class- and condition-specific mortality probabilities for Southern Resident killer whales (all pods combined). Calf and Juvenile age classes include both sexes. Violin plots represent the posterior distributions of the baseline age- and sex-specific mortality probabilities (top) and the effects of body condition class on mortality probability (bottom). Inset boxplots represent the median (black horizontal bar), 50% HPDI (white box), and 95% HPDI (vertical black lines). Note that the effects are estimated (and represented here) in logit space before transformation to proportional space. See Table 2 for estimated mortality probabilities of each age/sex and body condition class combination.

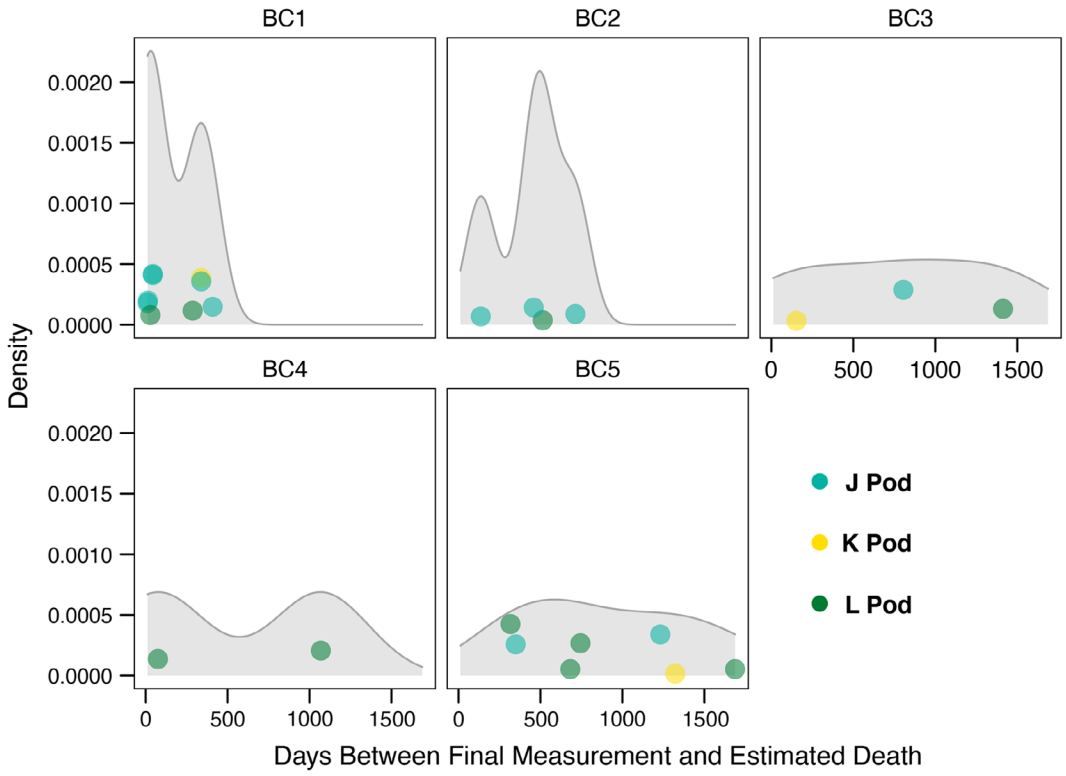

Fig. 4. Time between final condition measurement and estimated death for Southern Resident killer whales that died during the 2008–2019 study period. Each density plot represents the estimated number of days between when a whale was last measured and when it died, broken out by the condition class (BC1–5) that whales were last recorded as before death. Points represent the time between final measurement and death for individual whales, color coded by pod and jittered randomly on the *y*-axis.

covariates, given the ability of long-lived animals such as killer whales to live through bottlenecks in resource availability. In addition, there may be inherent differences in baseline condition between individuals, so evaluating individual changes between years rather than raw condition further accounts for individual variability.

Our cross-validation analyses suggest that, in the case of J and L pods, models including salmon covariates better predicted held-out years of body condition data than models without salmon covariates. Given that salmon managers use the FRAM model to generate pre-season estimates of Chinook abundance by stock, the modeling framework we present here could be used to generate predictions of fall SRKW body condition based on those salmon abundance estimates, quantify short-term risks to the population, and identify potential management interventions. Our model results suggest the strongest correlation between killer whale body condition and prey is between the SRKW J pod and Chinook salmon returning to the Fraser River. The Salish Sea area-based Chinook index was essentially tied for the best-fit J pod model, which is unsurprising considering the Salish Sea index is typically made up of 40–50% Fraser-origin Chinook. Over the last decade, when Fraser River Chinook abundance was above 750,000 (estimated FRAM Chinook model abundance on July 1st), J pod whales had a low chance (<14%) of declining body condition. Such a target could be used in a management setting to define thresholds supporting the stability and recovery of this population segment. For example, management actions focused on habitat restoration that ensures effective anadromous migration and productivity of Fraser River Chinook stocks could lead to gains

in the nutritive condition of J pod whales. In the long-term, increasing urbanization of watersheds (Greene and Beechie 2004), increasing abundance of competing predators (Chasco et al. 2017), interspecific competition with other salmon stocks (Losee et al. 2019, Kendall et al. 2020), and climate change (Crozier et al. 2008) all present substantial threats to Fraser River Chinook abundance.

The only positive, ecologically plausible relationship we found for L pod body condition was with the Puget Sound tributary-specific abundance index. This is surprising, given that L pod is rarely in Puget Sound in the summer and spends less time in adjacent inland waters during the summer months than J or K pods (Riera et al. 2019), and Puget Sound origin Chinook are generally smaller and less numerically dominant than other stocks (O'Neill et al. 2014, Pacific Fishery Management Council 2020). However, L pod spends more time during the summer months in the western strait of Juan de Fuca than J or K pods (Riera et al. 2019) and may be targeting Puget Sound Chinook as they migrate from their open ocean phase toward spawning tributaries. The somewhat unique oceanic distribution of Puget Sound Chinook along the west coast of Vancouver Island (Weitkamp 2010, Shelton et al. 2019) may provide a reliable prey base in areas or times when more dominant stocks (Columbia and Fraser rivers) are less abundant. The relationship between L pod body condition transitions and Puget Sound Chinook abundance was weaker than the relationship between J pod and Fraser River Chinook. It is possible that L pod targets Chinook from a variety of stocks as they enter the strait of Juan de Fuca, which could obscure the signal of the Puget Sound Chinook's influence on L pod body condition. However, L pod body condition was negatively correlated with all other tributary-specific and area-based indices, including all Chinook salmon present in the Southwest Vancouver Island region, which presumably would be a better representation of Chinook availability at the mouth of the strait of Juan de Fuca. Previous analyses examining the influence of specific Chinook stocks on SRKW demographic rates found a significant relationship between SRKW fecundity and both Puget Sound and Fraser River Chinook abundance (Vélez-Espino et al. 2014, Wasser et al. 2017), which further indicates the potential importance of these stocks to the SRKW population.

We focused our modeling efforts on Chinook salmon given their majority representation in SRKW diets during the summer months prior to our September condition measurements, but we note that other salmon species such as Coho may also be important to SRKW condition at other times of the year (Hanson et al. 2010, Ford et al. 2016). As photogrammetry measurements become available over a longer time period and throughout the year, it may be possible to extend this approach to evaluate the importance of other prey species and stocks on SRKW condition, including seasonal fluctuations in condition between late summer and spring (Fearnbach et al. 2020). Pink salmon have also been proposed as a possible driver of a reported biennial pattern of births and mortality in the SRKW population (Ruggerone et al. 2019). While pink salmon are not a known prey species for SRKW, the authors hypothesized that high densities of pink salmon returning in odd years could interfere with the ability of SRKW to target lower density Chinook, potentially explaining reduced fecundity and increased mortality in even years. There is some evidence of declines in SRKW condition in odd years, particularly in L pod (Appendix S1: Fig. S6), which may lend support to the foraging interference hypothesis and should be further explored as more data become available.

The best-fit model for K pod had fixed body condition transition probabilities across time and included no salmon covariate. While the abundance of K pod is lower than J or L pods, the proportion of K pod with condition measurements each year was high (Table 2), and we therefore do not consider small sample size to be a likely explanation for the absence of covariates in the best-fit model. K pod may forage on a diverse assemblage of prey that is not easily captured in either tributary-specific or area-based indices of Chinook abundance. However, the second best-fit model for K pod included Puget Sound Chinook and suggested a positive relationship between Chinook abundance and the probability of increasing body condition. Additional studies of the fine scale distribution of Puget Sound Chinook along Vancouver Island and the Washington coast, and their representation in the diets of L and K pod whales during summer months

Table 2. Number of Southern Resident killer whales measured using aerial photogrammetry in September of each study year, and the percentage of each pod imaged in parentheses.

Year	J pod	K pod	L pod
2008	23 (92.0)	18 (94.7)	19 (46.3)
2013	25 (96.2)	18 (94.7)	25 (67.6)
2015	27 (100)	19 (100)	26 (74.3)
2016	28 (96.6)	19 (100)	35 (100)
2017	22 (91.7)	9 (50.0)	30 (85.7)
2018	23 (100)	18 (100)	29 (85.3)
2019	22 (100)	17 (100)	21 (61.8)

could improve our understanding of the importance of this stock to SRKW population health. The major caveat to our findings is that body condition is known to fluctuate over a period of several months (Fearnbach et al. 2020). The three SRKW pods forage on other salmon stocks in winter and spring months (Hanson et al. 2010), but the September body condition metrics, and therefore the results of our analyses, most likely reflect the effects of the summer foraging period in the Salish Sea. Given the previously recorded increase in body condition from May to September and decline from September to May (Fearnbach et al. 2020), we posit that SRKW may have limited foraging opportunities over the winter and spring months, and that summer foraging in the Salish Sea may be the greatest driver of interannual body condition changes. However, SRKW may experience acute nutritional stress during winter and early spring when prey availability is restricted. Extending photogrammetry data collection throughout the year will help identify seasonal patterns in body condition fluctuations and may allow for comparative studies on the importance of winter/spring versus summer prey availability to SRKW health, survivorship, and reproductive success.

In addition to demonstrating the link between salmon abundance and body condition of killer whales, our model results show that whales in poor condition are more likely to die. Our estimated baseline mortality rates of whales in different age and sex classes are generally in line with previous findings (Ward et al. 2013), with old males and females experiencing the highest mortality probabilities, and calves experiencing slightly elevated mortality probabilities compared to juveniles and young whales. Our model estimated somewhat higher mortality probabilities for old females, and lower for old males, calves, and juveniles than previous analyses (Ward et al. 2013). These small differences are most likely due to the shorter time series of deaths included in our study (2008–2019 vs. 1979–2010) and the exclusion of whales that did not have body condition measurements, although we cannot rule out changes in mortality probability by age and sex class in recent years. Whales in condition class 1 had a mortality probability roughly 2–3 times higher than whales in condition classes 2–5. Interestingly, condition class 5 whales had a slightly elevated mortality probability similar to condition class 2 whales. The two whales that were observed in condition class 5 at the time step immediately prior to death died 317 (L53) and 349 (J14) days after being imaged and may have experienced a substantial, unrecorded decline in condition during that almost year-long period. Furthermore, while we did account for age and sex effects on mortality probability, there are other factors aside from age, sex, and nutritive condition that may contribute to mortality probabilities, such as the presence or condition of other whales in a matriline (Foster et al. 2012, Nattrass et al. 2019). The majority of whales that died shortly after being imaged were in condition class 1 (very poor condition), while deaths of higher condition class whales typically occurred longer after their last measurement (Fig. 4). During the study period, six whales in our photogrammetry dataset (J17, J28, J50, J52, J54, and L67) were also recorded from boat-based observations with a peanut head appearance, exhibiting severely depleted post-cranial fat stores (Fearnbach et al. 2018). All six of these whales were categorized as condition class 1 based on aerial photogrammetry measurements, and all of them died within one year of measurement (most within two months). This suggests agreement between these two indicators of terminal condition in killer whales. However, three additional condition class 1 whales died within a year after measurement and were not recorded as peanut heads (K25, J8, and L92). Aerial photogrammetry provides a quantitative—rather than subjective—and potentially more sensitive metric that can detect declines in condition and identify at-risk whales prior to the

terminal peanut head phase that is detectable from boat-based observations.

Interestingly, changes in condition for animals from J and L pod were best explained by Chinook indices that are asynchronous (Fraser River and Puget Sound; Appendix S1: Fig. S4), while K pod condition was best explained by constant transition probabilities (or possibly Puget Sound Chinook, similar to L pod). Our findings suggest that the three pods behave differently in terms of body condition fluctuations, which may be driven by independent foraging strategies. Recent analyses of SRKW demographic data attempted to relate births and deaths to a wide range of Chinook salmon area-based indices (including several of the area-based indices used in this study), but found no significant relationships (Pacific Fishery Management Council 2020). Our results indicate that it may be advantageous for similar future analyses of demographic fluctuations to consider the three SRKW pods separately. Furthermore, given the differences in important prey indices reported here, it may be more effective for management strategies to treat the population of SRKWs as multiple management units, as the most effective management actions may be different for each pod based on our findings.

In addition to identifying target prey abundance levels to support SRKW recovery, aerial photogrammetry can provide an early-warning system that has the potential to serve as the basis for dynamic and adaptive management strategies. In an endangered population that had only 73 remaining individuals as of 2019, demographic casualties such as the death of a reproductive female or a year with no successful births can potentially have catastrophic consequences for population viability. Management actions that respond to these demographic casualties, as opposed to preventing them, may be insufficient to support population recovery. Our findings show that aerial photogrammetry can be used to identify at-risk individual whales, as well as to collect an overall metric of population health prior to mortality events that could be used to inform management actions. For example, if a large portion of the population is recorded in body condition class 1 during September (e.g., more than 20% of the population, or some threshold decided upon by managers), then fishery actions could be considered to increase prey availability for SRKW pods over the next year. Assessments of condition could be done in near-real time with a lag of <3 months, rapidly informing upcoming management strategies or allowing for interventions at the individual level. Short-term actions that may result in an increase in Fraser Chinook abundance and accessibility include spatiotemporal closures in areas of high Fraser Chinook encounter rates or mark-selective regulations, as a high proportion of the Fraser stock aggregate is unmarked; and regulations such as vessel noise caps and revised vessel traffic regulations to reduce underwater noise and improve SRKW foraging success (Joy et al. 2019). Longer term proactive strategies to increase Chinook abundance could include habitat restoration and increased hatchery production (Greene and Beechie 2004, Crozier et al. 2008).

In addition to influencing survivorship, body condition is likely also tied to fecundity in killer whales (Ward et al. 2009, Wasser et al. 2017). Future work should examine the relationship between reproductive success in the SRKW population and observed body condition, which would allow for a full evaluation of the influence of individual condition on overall population viability and support further modeling and projection efforts to weigh the efficacy of candidate management strategies. In addition, monitoring body condition in other seasons could provide insights into prey populations that may be important to the SRKW population in winter and spring months. As the time series of condition measurements grows, it may be possible to evaluate the relationship between SRKW condition and finer scale Chinook stock groupings and other prey species.

It may not be possible to apply the approach used in this study to larger, more widely ranging populations of marine mammals where repeated measurements of individuals and samples from a large portion of the population are not feasible. Instead, the average body condition of a random sample of the population may be achievable and, based on our findings, can likely serve as a proxy for short-term, relative population health. In addition, we posit that rapid changes in average body condition within a population can be used as an early-warning indicator of upcoming

demographic fluctuations, given our findings that individuals in poor condition have higher mortality probabilities. The use of body condition as an indicator of population health shows promise for use in cetacean populations that have long-term photogrammetry datasets and experience substantial population fluctuations, such as eastern north Pacific gray whales (Perryman and Lynn 2002, Christiansen et al. 2020), which may help validate its use as a preceding signal of demographic impacts and support the development of adaptive management strategies.

Acknowledgments

Aerial and boat-based operations around whales were conducted under the authority of National Marine Fisheries Service Permits 532-1822, 16163, and 19091 in US waters and Species-At-Risk Act Permit 13-278 in Canada. Field operations and data analysis were conducted with funding support from the National Fish and Wildlife Foundation, the National Oceanographic and Atmospheric Administration (NOAA), the U.S. Fish and Wildlife Service, Shell, SeaWorld, SR3, NOAA Office of Marine and Aviation Operations (OMAO), NOAA/NMFS Office of Science and Technology, the Ocean Wise Conservation Association and the SeaWorld and Busch Gardens Conservation Fund. We are thankful to Lynne Barre for her support and encouragement and to Chris Yates and Lisa Ballance for their role in acquiring NOAA funds to support analysis. We thank Ken Balcomb for access to killer whale census data from the Center for Whale Research. We are also grateful to Ken Balcomb, Dave Ellifrit, Jane and Tom Cogan, Mark Malleson, Jessica Farrer, and Dylan Jones for their assistance with field operations, Molly Groskreutz and Alyssa Paredes for their efforts with photogrammetry analysis, and Wayne Perryman, Don LeRoi, and the NOAA/OMAO Aircraft Operations Center for their support for drone flight operations. This research was performed while JDS held an NRC Research Associateship award at the NOAA Southwest Fisheries Science Center. PKC held a contract with Ocean Associates, Inc. in support of the Marine Mammal and Turtle Division, Southwest Fisheries Science Center. The views and conclusions contained in this document are those of the authors and should not be interpreted as representing the opinions of policies of the U.S. Government or the National Fish and Wildlife Foundation and its funding sources. Mention of trade names or commercial products does not constitute their endorsement by the U.S. Government, or the National Fish and Wildlife Foundation or its funding sources. Author contributions are as follows: JDS: analysis conceptualization, data analysis, manuscript writing and editing; JWD: study conceptualization, funding acquisition, data collection and analysis, manuscript editing; HF: study conceptualization, funding acquisition, data collection and analysis, manuscript editing; LGBL: funding acquisition, data collection, manuscript editing; PKC: data analysis, manuscript editing; EJW: data analysis, manuscript editing; DRD: data analysis, manuscript editing.

Literature Cited

Berger, J. 2012. Estimation of body-size traits by photogrammetry in large mammals to inform conservation. Conservation Biology 26:769–777.

Boulanger, J., M. Cattet, S. E. Nielsen, G. Stenhouse, and J. Cranston. 2013. Use of multi-state models to explore relationships between changes in body condition, habitat and survival of grizzly bears *Ursus arctos horribilis*. Wildlife Biology 19:274–288.

Brosi, B. J., and E. G. Biber. 2009. Statistical inference, type II error, and decision making under the US endangered species act. Frontiers in Ecology and the Environment 7:487–494.

Center for Whale Research. 2020. Annual SRKW demographic data. Center for Whale Research, Friday Harbor, San Juan Island, Washington, USA.

Chasco, B., et al. 2017. Estimates of Chinook salmon consumption in Washington State inland waters by four marine mammal predators from 1970 to 2015. Canadian Journal of Fisheries and Aquatic Sciences 74:1173–1194.

Christiansen, F., A. M. Dujon, K. R. Sprogis, J. P. Y. Arnould, and L. Bejder. 2016. Noninvasive unmanned aerial vehicle provides estimates of the energetic cost of reproduction in humpback whales. Ecosphere 7:1–18.

Christiansen, F., F. Rodríguez-González, S. Martínez-Aguilar, J. Urbán, S. Swartz, H. Warick, F. Vivier, and L. Bejder. 2020. Poor body condition associated with an unusual mortality event in gray whales. Marine Ecology Progress Series 658:237–252.

Christiansen, F., F. Vivier, C. Charlton, R. Ward, A. Amerson, S. Burnell, and L. Bejder. 2018. Maternal body size and condition determine calf growth rates in Southern right whales. Marine Ecology Progress Series 592:267–282.

Cobb, G. W., and Y.-P. Chen. 2003. An application of Markov Chain Monte Carlo to community ecology. The American Mathematical Monthly 110:265–288.

Crozier, L. G., R. W. Zabel, and A. F. Hamlet. 2008. Predicting differential effects of climate change at the population level with life-cycle models of spring Chinook salmon. Global Change Biology 14:236–249.

Dennis, B. 1989. Allee effects: population growth, critical density, and the chance of extinction. Natural Resource Modeling 3:481–538.

Durban, J. W., H. Fearnbach, L. G. Barrett-Lennard, W. l. Perryman, and D. J. Leroi. 2015. Photogrammetry of killer whales using a small hexacopter launched at sea. Journal of Unmanned Vehicle Systems 3:131–135.

Fearnbach, H., J. W. Durban, L. G. Barrett-Lennard, D. K. Ellifrit, and K. C. Balcomb. 2020. Evaluating the power of photogrammetry for monitoring killer whale body condition. Marine Mammal Science 36:359–364.

Fearnbach, H., J. W. Durban, D. K. Ellifrit, and K. C. Balcomb. 2011. Size and long-term growth trends of endangered fish-eating killer whales. Endangered Species Research 13:173–180.

Fearnbach, H., J. W. Durban, D. K. Ellifrit, and K. C. Balcomb. 2018. Using aerial photogrammetry to detect changes in body condition of endangered southern resident killer whales. Endangered Species Research 35:175–180.

Ford, J. K. B., G. M. Ellis, L. G. Barrett-Lennard, A. B. Morton, R. S. Palm, and K. C. Balcomb. 1998. Dietary specialization in two sympatric populations of killer whales (*Orcinus orca*) in coastal British Columbia and adjacent waters. Canadian Journal of Zoology 76:1456–1471.

Ford, J. K. B., G. M. Ellis, P. F. Olesiuk, and K. C. Balcomb. 2010. Linking killer whale survival and prey abundance: food limitation in the oceans' apex predator? Biology Letters 6:139–142.

Ford, M. J., J. Hempelmann, M. B. Hanson, K. L. Ayres, R. W. Baird, C. K. Emmons, J. I. Lundin, G. S. Schorr, S. K. Wasser, and L. K. Park. 2016. Estimation of a killer whale (*Orcinus orca*) population's diet using sequencing analysis of DNA from feces. PLOS ONE 11:1–14.

Foster, E. A., D. W. Franks, S. Mazzi, S. K. Darden, K. C. Balcomb, J. K. B. Ford, and D. P. Croft. 2012. Adaptive prolonged postreproductive life span in killer whales. Science 337:1313.

Gelman, A., and D. B. Rubin. 1992. Inference from iterative simulation using multiple sequences. Statistical Science 7:457–472.

Goebel, M. E., W. L. Perryman, J. T. Hinke, D. J. Krause, N. A. Hann, S. Gardner, and D. J. LeRoi. 2015. A small unmanned aerial system for estimating abundance and size of Antarctic predators. Polar Biology 38:619–630. https://doi.org/10.1007/s00300-014-1625-4

Greene, C. M., and T. J. Beechie. 2004. Consequences of potential density-dependent mechanisms on recovery of ocean-type chinook salmon (*Oncorhynchus tshawytscha*). Canadian Journal of Fisheries and Aquatic Sciences 61:590–602.

Groskreutz, M., J. Durban, H. Fearnbach, L. Barrett-Lennard, J. Towers, and J. Ford. 2019. Decadal changes in adult size of salmon-eating killer whales in the eastern North Pacific. Endangered Species Research 40:183–188.

Hanson, M. B., et al. 2010. Species and stock identification of prey consumed by endangered southern resident killer whales in their summer range. Endangered Species Research 11:69–82.

Hu, J., X. Wu, and M. Dai. 2020. Estimating the population size of migrating Tibetan antelopes *Pantholops hodgsonii* with unmanned aerial vehicles. Oryx 54:101–109.

Huggins, J. L., M. M. Garner, S. A. Raverty, D. M. Lambourn, S. A. Norman, L. D. Rhodes, J. K. Gaydos, J. K. Olson, M. Haulena, and M. B. Hanson. 2020. The emergence of mucormycosis in free-ranging marine mammals of the Pacific Northwest. Frontiers in Marine Science 7:1–9.

Joy, R., D. Tollit, J. Wood, A. MacGillivray, Z. Li, K. Trounce, and O. Robinson. 2019. Potential benefits of vessel slowdowns on endangered southern resident killer whales. Frontiers in Marine Science 6:1–20.

Kendall, N. W., B. W. Nelson, and J. P. Losee. 2020. Density-dependent marine survival of hatchery-origin Chinook salmon may be associated with pink salmon. Ecosphere 11:1–20.

Kery, M., and M. Schaub 2012. Bayesian population analysis using WinBUGS: a hierarchical perspective. Elsevier, Amsterdam, The Netherlands.

Krahn, M. M., M. B. Hanson, G. S. Schorr, C. K. Emmons, D. G. Burrows, J. L. Bolton, R. W. Baird, and G. M. Ylitalo. 2009. Effects of age, sex and reproductive status on persistent organic pollutant concentrations in "Southern Resident" killer whales. Marine Pollution Bulletin 58:1522–1529.

Liu, D., K. Song, J. R. G. Townshend, and P. Gong. 2008. Using local transition probability models in Markov random fields for forest change detection. Remote Sensing of Environment 112:2222–2231.

Losee, J. P., N. W. Kendall, and A. Dufault. 2019. Changing salmon: an analysis of body mass, abundance, survival, and productivity trends across 45 years in Puget Sound. Fish and Fisheries 20:934–951.

Lundin, J. I., et al. 2016. Modulation in persistent organic pollutant concentration and profile by prey availability and reproductive status in southern resident killer whale scat samples. Environmental Science and Technology 50:6506–6516.

Lusseau, D., D. E. Bain, R. Williams, and J. C. Smith. 2009. Vessel traffic disrupts the foraging behavior of southern resident killer whales *Orcinus orca*. Endangered Species Research 6:211–221.

Mitchell, T. J., and J. J. Beauchamp. 1988. Bayesian variable selection in linear regression. Journal of the American Statistical Association 83:1023–1032.

National Marine Fisheries Service. 2019. Killer whale (*Orcinus orca*): Eastern North Pacific Southern Resident Stock. NOAA Marine Mammal Stock Assessment. National Marine Fisheries Service, Silver Spring, Maryland, USA.

Nattrass, S., et al. 2019. Postreproductive killer whale grandmothers improve the survival of their grandoffspring. Proceedings of the National Academy of Sciences of the United States of America 116:26669–26673.

O'Neill, S. M., G. M. Ylitalo, and J. E. West. 2014. Energy content of Pacific salmon as prey of northern and southern resident killer whales. Endangered Species Research 25:265–281.

Pacific Fishery Management Council. 2008. Fishery Regulation Assessment Model (FRAM) - an overview for Coho and Chinook - v 3.0. Pacific Fishery Management Council, Portland, Oregon, USA.

Pacific Fishery Management Council. 2020. Pacific Fishery Management Council Salmon Fishery Management Plan Impacts to Southern Resident Killer Whales. Pacific Fishery Management Council, Portland, Oregon, USA.

Parsons, K. M., K. C. Balcomb, J. K. B. Ford, and J. W. Durban. 2009. The social dynamics of southern resident killer whales and conservation implications for this endangered population. Animal Behaviour 77:963–971.

Perryman, W. L., and M. S. Lynn. 2002. Evaluation of nutritive condition and reproductive status of migrating gray whales (*Eschrichtius robustus*) based on analysis of photogrammetric data. Journal of Cetacean Research and Management 4:155–164.

Plummer, M. 2003. JAGS: a program for analysis of Bayesian graphical models using Gibbs sampling. In Proceedings of the 3rd international workshop on distributed statistical computing 124.

R Core Team. 2016. R: a language and environment for statistical computing. R Foundation for Statistical Computing, Vienna, Austria.

Raverty, S., et al. 2020. Pathology findings and correlation with body condition index in stranded killer whales (*Orcinus orca*) in the northeastern Pacific and Hawaii from 2004 to 2013. PLOS ONE 15: e0242505.

Riera, A., J. F. Pilkington, J. K. B. Ford, E. H. Stredulinsky, and N. R. Chapman. 2019. Passive acoustic monitoring off Vancouver Island reveals extensive use by at-risk Resident killer whale (*Orcinus orca*) populations. Endangered Species Research 39:221–234.

Ruckelshaus, M. H., P. Levin, J. B. Johnson, and P. M. Kareiva. 2002. The Pacific salmon wars: what science brings to the challenge of recovering species. Annual Review of Ecology and Systematics 33:665–706.

Ruggerone, G. T., A. M. Springer, L. D. Shaul, and G. B. Van Vliet. 2019. Unprecedented biennial pattern of birth and mortality in an endangered apex predator, the southern resident killer whale, in the eastern North Pacific Ocean. Marine Ecology Progress Series 608:291–296.

Schönbrodt, F. D., and M. Perugini. 2013. At what sample size do correlations stabilize? Journal of Research in Personality 47:609–612.

Sheer, M. B., and E. A. Steel. 2006. Lost watersheds: barriers, aquatic habitat connectivity, and salmon persistence in the Willamette and Lower Columbia River Basins. Transactions of the American Fisheries Society 135:1654–1669.

Shelton, A. O., W. H. Satterthwaite, E. J. Ward, B. E. Feist, and B. Burke. 2019. Using hierarchical models to estimate stock-specific and seasonal variation in ocean distribution, survivorship, and aggregate abundance of fall run chinook salmon. Canadian Journal of Fisheries and Aquatic Sciences 76:95–108.

Soulé, M. E., editor. 1987. Viable populations for conservation. Cambridge University Press, Cambridge, UK.

Vehtari, A., A. Gelman, and J. Gabry. 2017. Practical Bayesian model evaluation using leave-one-out cross-validation and WAIC. Statistics and Computing 27:1413–1432.

Vélez-Espino, L. A., J. K. B. Ford, H. A. Araujo, G. Ellis, C. K. Parken, and R. Sharma. 2014. Relative importance of chinook salmon abundance on resident killer whale population growth and viability. Aquatic Conservation: marine and Freshwater Ecosystems 25:756–780.

Vindenes, Y., E. Edeline, J. Ohlberger, Ø. Langangen, I. J. Winfield, N. C. Stenseth, and L. Asbjørn Vøllestad. 2014. Effects of climate change on trait-based dynamics of a top predator in freshwater ecosystems. American Naturalist 183:243–256.

Walsh, P. D. 2000. Sample size for the diagnosis of conservation units. Conservation Biology 14:1533–1537.

Ward, E. J., M. J. Ford, R. G. Kope, J. K. B. Ford, L. A. Velez-Espino, C. K. Parken, L. W. LaVoy, M. B. Hanson and K. C. Balcomb. 2013. Estimating the impacts of Chinook salmon abundance and prey removal by ocean fishing on Southern Resident

killer whale population dynamics. NOAA technical memorandum NMFS-NWFSC-123. U.S. Department of Commerce.

Ward, E. J., E. E. Holmes, and K. C. Balcomb. 2009. Quantifying the effects of prey abundance on killer whale reproduction. Journal of Applied Ecology 46:632–640.

Wasser, S. K., J. I. Lundin, K. Ayres, E. Seely, D. Giles, K. Balcomb, J. Hempelmann, K. Parsons, and R. Booth. 2017. Population growth is limited by nutritional impacts on pregnancy success in endangered Southern Resident killer whales (*Orcinus orca*). PLOS ONE 12:e0179824.

Weitkamp, L. A. 2010. Marine distributions of chinook salmon from the West Coast of North America determined by coded wire tag recoveries. Transactions of the American Fisheries Society 139:147–170.

Welch, D. W., A. D. Porter, and E. L. Rechisky. 2021. A synthesis of the coast-wide decline in survival of West Coast Chinook Salmon (*Oncorhynchus tshawytscha*, Salmonidae). Fish and Fisheries 22:194–211.

Wood, S. N. 2006. Generalized additive models: an introduction with R. Chapman and Hall, Boca Raton, Florida, USA.

Data Availability

Data and code to run multi-state models can be found at: https://github.com/stewart6/SRKW-MultiState

Supporting Information

Additional Supporting Information may be found online at: http://onlinelibrary.wiley.com/doi/10.1002/ecs2.3660/full